APRIL 09 2009

Microbubble tunneling in gel phantoms

Charles F. Caskey; Shengping Qin; Paul A. Dayton; Katherine W. Ferrara

J. Acoust. Soc. Am. 125, EL183–EL189 (2009)
https://doi.org/10.1121/1.3097679

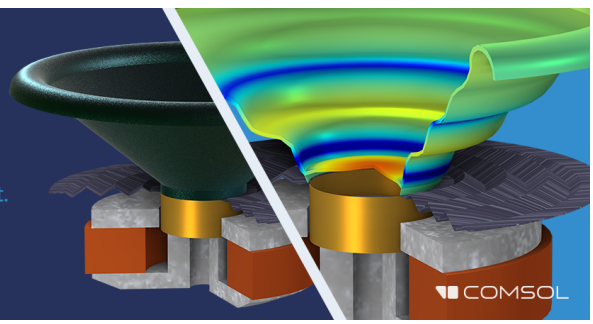

Microbubble tunneling in gel phantoms

Charles F. Caskey and Shengping Qin
Department of Biomedical Engineering, University of California, Davis, 451 East Health Sciences Drive, Davis, California 95616
cfcaskey@ucdavis.edu, spqin@ucdavis.edu

Paul A. Dayton
Joint Department of Biomedical Engineering, University of North Carolina–North Carolina State University, Chapel Hill, North Carolina 27514
padayton@bme.unc.edu

Katherine W. Ferrara
Department of Biomedical Engineering, University of California, Davis, 451 East Health Sciences Drive, Davis, California 95616
kwferrar@ucdavis.edu

Abstract: Insonified microbubbles were observed in vessels within a gel with a Young's modulus similar to that of tissue, demonstrating shape instabilities, liquid jets, and the formation of small tunnels. In this study, tunnel formulation occurred in the direction of the propagating ultrasound wave, where radiation pressure directed the contact of the bubble and gel, facilitating the activity of the liquid jets. Combinations of ultrasonic parameters and microbubble concentrations that are relevant for diagnostic imaging and drug delivery and that lead to tunnel formation were applied and the resulting tunnel formation was quantified.

PACS numbers: 43.80.Gx [TM]
Date Received: December 5, 2008 **Date Accepted:** February 2, 2009

Our laboratory and others have previously shown that upon insonation of a region of interest, microbubble oscillations within vessels with diameters as large as 55 μm can substantially increase vascular permeability and cause local hemorrhage.[1–3] Recent studies have helped elucidate the parameter space for enhancing permeability and avoiding injury by indirect observation of biological effects (magnetic resonance imaging signal enhancement[4] and hemorrhage counts[5]). The current work examines a similar parameter space but focuses on direct observation of microbubble oscillations and the resulting disruption of a gel that has a Young's modulus similar to soft tissues. As an initial effort to identify the mechanisms of gel disruption, bubble oscillation characteristics are then compared to theoretical predictions of bubble oscillation and collapse using simplified models.

Microbubbles in a gel flow phantom were observed during a 20-s insonation with frequencies of 1, 2.25, and 5 MHz using one of two combinations for pulse repetition frequency (PRF) and pulse duration (PD), chosen to simulate either common imaging ($PD_{image}=10$ μs, $PRF_{image}=10$ kHz) or drug delivery parameters ($PD_{delivery}=10$ ms, $PRF_{delivery}=10$ Hz) with matched time-averaged intensity. The center frequencies and peak negative pressure (PNP) examined were chosen to investigate the ranges used for drug delivery (0.26–2.5 MHz, PNP >0.64 MPa).[2,6]

The ultrasound system consists of an ultrasound source, spherically focused and aligned so that the acoustic field and observation area overlapped. The gel phantom was a small block ($30\times20\times2$ mm^3) of 0.75% (w/v) OmniPur agarose gel (EM Science, Gibbstown, NJ) with an embedded 230-μm channel created by a heating and cooling process.[7] The channel size is the smallest diameter that can be easily perfused with microbubbles within our gel phantom. At 0.75% (w/v), the phantom is estimated to have a Young's modulus in the range of 10–20 kPa, which is similar to soft tissues in biological systems, such as the kidneys, liver, and muscle.[7,8]

Lipid-shelled microbubbles were made using techniques described previously.[9] The concentration of microbubbles was approximately 1.5×10^{10} bubbles/ml, with a mean diameter of 1.7 ± 1.6 μm. The solution was diluted in distilled water so that the final solution ranged from the dosage used for diagnostic therapy ($\sim1.6\times10^{5}$ bubbles/ml) to high dosages used in many drug delivery experiments ($\sim2.5\times10^{7}$ bubbles/ml). A perfusion pump was set so that the flow rate within the vessel was approximately 36 mm/s. After insonation, a solution of blue 500-nm microbeads (Polysciences, Warrington, PA) was injected to delineate wall boundaries within the gel. High-speed strobe images were captured by synchronizing a pulsed copper vapor laser (30-ns pulse width) to a camera with a 10-kHz frame rate. The laser flash created an effective exposure time of 30 ns to capture microbubble oscillation activity during the time that the shutter was open (0.1 ms). The laser was pulsed at 9.997 kHz to achieve an incremental delay of 30 ns during the 10-ms acoustic pulse, which allowed us to visualize the bubble oscillation during the positive and negative cycles of the acoustic pulse.[10] Disruption of the vessel wall was quantified by measuring the width and depth of tunnels formed. Bubble diameter was measured after the onset of tunnel formation and used as an input to a model of bubble oscillation. In order to correlate the tunnel width to the bubble oscillation, a Rayleigh–Plesset-based model[11] was used to predict the maximum bubble expansion. A similar form of the Rayleigh–Plesset-based equation has been used to simulate a bubble surrounded by a soft gel during insonation.[12] For simplicity, the terms representing the elastic/plastic properties of the gel have been neglected in our simulation.

The apparent threshold for tunnel formation for a given combination of transmission frequency and bubble concentration was determined by incrementing the PNP by 200 kPa until tunnel formation began. Threshold experiments were repeated five times for each combination of frequency and concentration to ensure accurate measurement. The effect of angle of insonation was analyzed by measuring the average direction of tunnel formation relative to ultrasound propagation. All image measurements were performed with IMAGEJ (NIH, http://rsb.info.nih.gov/ij/). Statistical analysis of tunnel widths was performed with the Student's *t*-test ($p=0.05$ indicates significance).

Figures 1(a)–1(c) show representative examples of tunnels formed in the gel during insonation at 1, 2.25, and 5 MHz, respectively, with a matched mechanical index (MI) of 1.5, PD of 10 ms, and a high bubble concentration (2.5×10^{7} bubbles/ml). The axis of the ultrasound beam was vertical and directed upward. The average widths of tunnels created by the bubbles during insonation at 1, 2.25, and 5 MHz were 39.7 ± 6.8, 21.8 ± 2.3, and 7.4 ± 1.5 μm, respectively. The decrease in tunnel width with increasing frequency was expected due to the decreased maximum microbubble diameter during oscillation. The maximum depth of tunnels created by bubbles in these experiments increased with decreasing ultrasound center frequency; the depths of the tunnels were 1.2 ± 0.52, 0.36 ± 0.16, and 0.15 ± 0.09 mm with center frequencies of 1, 2.25, and 5 MHz, respectively.

Asymmetrical oscillation after tunnel formation has begun was visualized in sequential high-speed strobe images acquired with high magnification [Figs. 1(d)–1(g)], using a center frequency of 1 MHz, a PNP of 1.2 MPa, the beam-vessel axis as in Figs. 1(a)–1(c), and a high microbubble concentration (2.5×10^{7} bubbles/ml). With these parameters, the PNP of 1.2 MPa is the threshold for tunnel creation in the agarose gel and is similar to the PNP previously determined during *in vivo* studies.[1] In the first image (1d), two microbubble clusters were shown just before coalescence. At a later point in time (1e), the recently formed microbubble has entered the tunnel. The bubble compressed to an undetectably small diameter during the positive phase of the ultrasonic pulse (1f). During a subsequent negative acoustic pressure phase (1g) the microbubble expanded to a diameter equal to the tunnel width. In this instance, the microbubble expanded to a diameter of 45 μm and translated a distance of 1.2 μm down the tunnel over the course of 10 ms (i.e., at a velocity of 1.2 mm/s). Since we observe that the microbubbles fully fill the tunnels at peak expansion, the tunnel width was representative of peak expansion, while the tunnel depth indicates repeated oscillation and persistence during a long ultrasonic pulse.

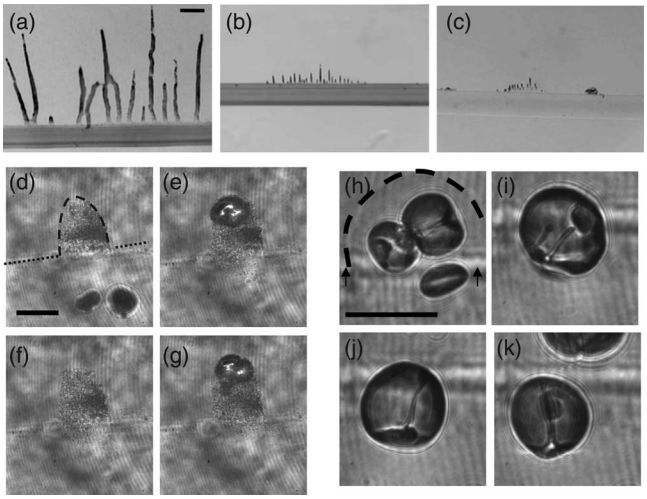

Fig. 1. Tunnel images and high-speed microscopy. Optical evidence of tunnel formation using a microbubble concentration of $\sim 2.5 \times 10^7$ bubbles/ml and pulse duration of 10 ms. Tunnels created from insonation at (a) 1-MHz, (b) 2.25-MHz, and (c) 5-MHz ultrasonic pulses at matched MI of 1.5. Scale bar indicates 250 μm. Sequential high-speed images (d)–(g) show a microbubble oscillating during a 1-MHz pulse creating a 45-μm-diameter tunnel. The frame rate is 10 kHz and the first image is acquired at 0.1 ms after the onset of insonation. Subsequent images were selected to show compressional and rarefactional half-cycles. The microbubble forms in (d) from the fusion of multiple microbubble fragments and then oscillates asymmetrically as it moves through the gel. Scale bar indicates 50 μm. High-speed images (h)–(k) show multi-bubble interactions and fluid jets during the formation of a 50-μm tunnel. The frame rate is 10 kHz and the images are selected for clear jet visualization. Scale bar indicates 50 μm.

While Figs. 1(d)–1(g) show significant events that occur during tunnel formation, including coalescence and expansion, higher magnification images were acquired to visualize fluid jets. Liquid jets are visible within each microbubble in Figs. 1(h)–1(k), which are a sequence of images acquired as a bubble enters a newly-formed tunnel. The arrows in Fig. 1(h) point to the boundary of the gel wall, which is evident in Figs. 1(h)–1(k) as a diffuse light horizontal line. The dotted line in Fig. 1(h) indicates the boundary of the tunnel that is being formed. The same tunnel is present but out of the frame in Figs. 1(i)–1(k). The images are similar to observations of fluid jets created by much larger bubbles (with diameters on the order of millimeters) that have been shown to disrupt gel boundaries.[13] The jets formed in various directions, as compared with the beam axis and surface normal, with jet neck diameters, r_j, ranging from 2 to 15 μm. Jets formed both in the presence [Figs. 1(h) and 1(k)] and absence [Figs. 1(i) and 1(j)] of surrounding bubbles and were observed to traverse the entire bubble diameter in some cases. As shown previously by other researchers, the wide range in jet diameter and direction is expected due to varied bubble size, the presence or absence of nearby bubbles, and the location of the bubble relative to the vessel wall during the acoustic pulse.[14] The pressure of a fluid jet impacting on a compressible solid boundary is

$$P_{WH} = \frac{\rho_1 c_1 \rho_2 c_2 v}{\rho_1 c_1 + \rho_1 c_1}, \tag{1}$$

where v is the velocity of the jet and $\rho_{1,}c_1$ and $\rho_{2,}c_2$ are the products of the densities and speed of sound in the water and gel boundary, respectively.[15] The duration of the jet impact is estimated to be

$$\tau_j = \frac{r_j}{c}. \quad (2)$$

Assuming that the density and speed of sound are not significantly different between the gel and water, we take the densities to be 997.99 kg m^{-3} and the sound velocities as 1485.9 m s^{-1}. For jet velocities similar to predicted wall velocity at collapse, the jet impact pressure will be in the range of hundreds of megapascals, with impact lasting between 1.3 and 10 ns. This pressure far exceeds the tensile strength of the gel which is about 0.056 MPa for a similar gel,[12] and therefore the observed jets are expected to play a role in tunnel formation.

The effect of PNP was next evaluated for center frequencies of 1 and 2.25 MHz at two concentrations (PD=10 ms and PRF=10 Hz). Tunnels were not observed for a PNP of 1 MPa or below for a center frequency of 1 MHz at either concentration. The PNP threshold for tunnel digging at 1 MHz was 1.2 MPa which is comparable to the regime where Prentice *et al.*[16] observed microjet phenomenon. Tunnels were not observed with insonation at 2.25 MHz using the contrast agent concentration used for diagnostic imaging. At the higher concentration and with insonation at 2.25 MHz, a trend of increasing tunnel width with increasing PNP was observed. With this higher concentration, the PNP threshold for tunnel creation was 0.6 MPa for the 2.25-MHz center frequency.

The higher concentration employed in the 2.25-MHz studies resulted in microbubble coalescence during the long pulses. After insonation, the diameters of microbubbles responsible for tunnel formation were optically measured, yielding a mean diameter of 9.3 ± 3.4 μm (where the mean diameter was ~ 1.7 μm before coalescence). Smaller bubbles typically dissolved during the ultrasonic pulse. Larger microbubbles (>10 μm) were observed to form from coalescence but oscillated with a low amplitude within the tunnel and did not disrupt the gel.

Predictions for the maximum diameter achieved during insonation at 1 and 2.25 MHz, respectively, for a microbubble with a diameter of 9.3 μm are shown by the dashed lines [Fig. 2(a)]. The maximum diameter of the tunnels formed increases with PNP, peaking at 47 and 25 μm for the 1- and 2.25-MHz center frequencies, respectively. While the inception of tunnel formation was a result of jet formation, the width of the tunnels approaches the width associated with maximum expansion (as shown in Fig. 1).

Decreasing the ultrasound center frequency increased tunnel width for a constant MI, as shown in Fig. 2(b) where the tunnel width was averaged over five observations for each center frequency tested (MI=1.2, 1.5). Thus, tunnel width exhibits a stronger dependence on transmission center frequency than that predicted by MI, as previously noted.[1,17] The predicted maximum bubble diameters during peak expansion for MI values of 1.2 and 1.5 [solid and dotted lines in Fig. 2(b)] indicate that the tunnel width was similar to the expected diameter of oscillating microbubbles.

When the PD was decreased from 10 ms to 10 μs (while increasing the PRF from 10 Hz to 10 kHz so that the time-averaged acoustic intensity was matched), the threshold for disrupting the gel wall increased from 1.2 to greater than 2.5 MPa at both low and high bubble concentrations. With the shorter pulse, diffusion of the gas bubble into the surrounding liquid may occur prior to the next pulse. A thorough investigation of the effect of pulse duration on gel disruption is underway.

Increasing microbubble concentration decreases the PNP threshold for gel disruption at transmission frequencies greater than or equal to 2.25 MHz (PRF of 10 Hz and PD of 10 ms) [Fig. 2(c)]. At 1 and 1.5 MHz, the threshold for gel disruption was similar across all concentrations investigated in our study. The effect on the gel wall became undetectable at diagnostic bubble concentrations (1.5×10^5 bubbles/ml) using transmission frequencies above 1.5 MHz for PNPs as high as 5 MPa.

In all cases examined, tunnels were formed on the distal side of the vessel relative to the ultrasound transducer; vessel wall damage was never observed on the side of the vessel proximal to the transducer. While in contact with the wall, the bubbles moved into the gel in the direction of the ultrasound propagation. The direction of the tunnel formation was the same as

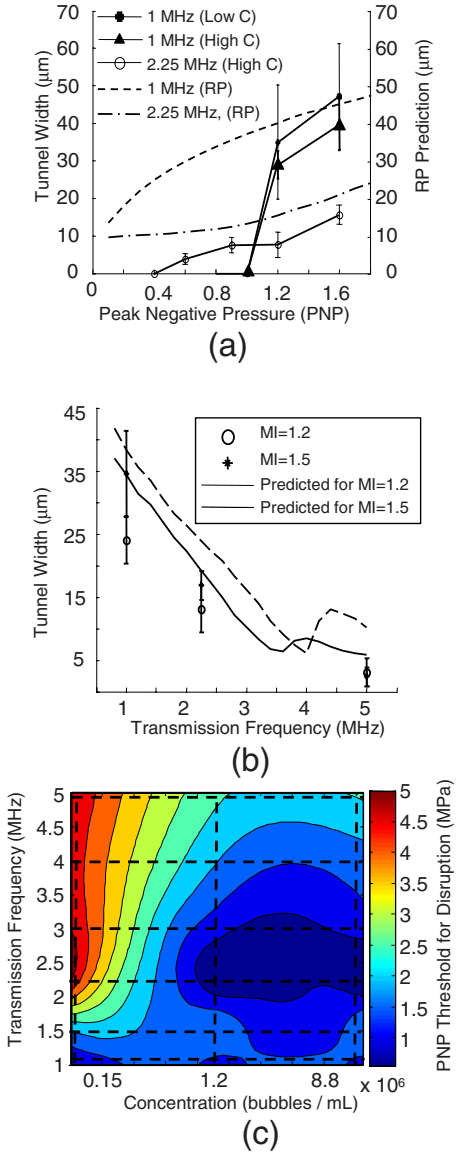

Fig. 2. (Color online) Tunnel formation and parameters. (a) Tunnel width for two transmission frequencies (1 and 2.25 MHz) and two concentrations (1.5×10^5 and 2.5×10^7 bubbles/ml) with a pulse duration of 10 ms; Rayleigh–Plesset predictions for maximum diameter of a microbubble in an infinite fluid. Tunnel width increases with PNP for 1 and 2.25 MHz at high bubble concentration, while tunnel formation at low concentration was only possible at 1 MHz. The lower threshold is indicated by the point where tunnel width is zero. At the higher pressures, tunnel width approaches the maximum diameter predicted by a 9.3-μm bubble (the diameter observed to interact with the wall). (b) Average tunnel width for three center frequencies using a matched MI, pulse duration of 10 ms, and microbubble concentration of 2.5×10^7 bubbles/ml. The solid and dashed lines in the plot indicate the predicted size of a 9.3-μm bubble according to simulation. (c) Surface fit indicating thresholds for tunnel formation as a function of frequency and bubble concentration. Intersection of dotted lines indicates a frequency and concentration combination tested.

that of ultrasound propagation, regardless of the angle of the vessel [Fig. 3(a)]. At vessel angles of 90, 75, and 60 degrees relative to the beam axis, the orientation of the tunnels formed was consistent with the direction of ultrasound propagation [Fig. 3(b)]. Primary radiation force maintains the bubble's contact with the wall and translates the bubble in the direction of ultra-

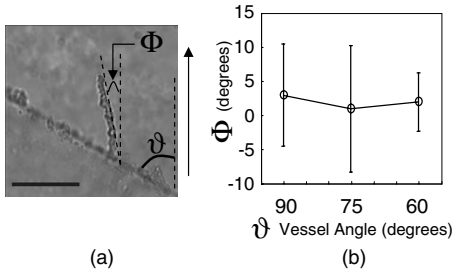

Fig. 3. Varying the beam-vessel angle. (a) With 2.25-MHz insonation (PNP of 1.2 MPa), pulse duration of 10 ms, and concentration of 2.5×10^7 bubbles/ml, representative image of tunnel formation vs beam direction indicated by arrow and vessel wall orientation shown as diagonal wall. (b) Summary of tunnel angle, Φ, and vessel angle, ϑ, each relative to the ultrasound beam for conditions summarized in (a). For vessel angles as small as 60° relative to the beam axis, the tunnel consistently forms in the same direction as the ultrasonic pulse.

sonic beam. We hypothesize that tunnel creation was likely due to a combination of fluid jets, bubble expansion, and primary radiation force during bubble oscillation.

Dayton *et al.*[18] calculated the magnitude of primary radiation force to be approximately 1×10^{-5} N for a bubble with an initial radius of 1.63 μm during a 2.25-MHz pulse (PNP = 100 kPa). In the present study, the PNP and PD are both substantially larger and the local stress due to radiation force is higher and the radiation force deflects bubbles along the beam axis (Fig. 3). After tunnel formation has begun, the microbubble is constrained by two nearby boundaries and its oscillation could expand against the surrounding tunnel, which is similar to a scenario previously examined,[17] where bubble expansion results in circumferential stress that can contribute to breakdown of the gel boundary.

The studies reported here demonstrate multiple factors that must be considered when designing safe diagnostic and drug delivery procedures using ultrasound contrast agents, including microbubble concentration, center frequency, acoustic pressure, and pulse duration. Observations reported here are similar to those reported previously for an *ex vivo* preparation, while allowing for easier quantification of bubble activity and associated acoustic parameters.[10] In the present study, a set of parameters was observed that does not result in tunnel formation, including a center frequency of 2.25 MHz (the threshold frequency was between 1 and 2.25 MHz) with a diagnostic concentration of small-lipid shelled microbubbles and a pressure up to 5 MPa. Alternatively, a high concentration of microbubbles and long pulse can produce an effect even with the 5-MHz center frequency. When the frequency was reduced to 1 MHz, tunnel formation was observed with both the diagnostic and therapeutic concentrations of microbubbles for either insonation with a long pulse (high duty cycle) and PNP above 1 MPa or a short (imaging pulse) and PNP above 2.5 MPa.

As in all phantom studies, this study has limitations that must be recognized in the interpretation of our results. First, while we seek to investigate a phantom capillary using a well-known concept (a tunnel within a gel), due to the logistics of the experiments, the vessel was larger than a typical capillary. Further, the basement membrane of a vessel may limit the depth of tunneling within a vessel. Alternatively, the studies facilitate an examination of the nucleation of small pores or tunnels and the interaction of the primary radiation pressure and microbubble collapse resulting in the translation of the microbubble in the direction of the radiation pressure.

Acknowledgments

The authors would like to acknowledge funding from NIH R01CA103828 and R01CA112356.

References and links

[1]S. M. Stieger, C. F. Caskey, R. H. Adamson, S. Qin, F. R. Curry, E. R. Wisner, and K. W. Ferrara, "Enhancement of vascular permeability with low-frequency contrast-enhanced ultrasound in the chorioallantoic membrane model," Radiology **243**, 112–121 (2007).

[2]D. L. Miller and J. Quddus, "Diagnostic ultrasound activation of contrast agent gas bodies induces capillary rupture in mice," Proc. Natl. Acad. Sci. U.S.A. **97**, 10179–10184 (2000).
[3]R. J. Price, D. M. Skyba, S. Kaul, and T. C. Skalak, "Delivery of colloidal particles and red blood cells to tissue through microvessel ruptures created by targeted microbubble destruction with ultrasound," Circulation **98**, 1264–1267 (1998).
[4]N. McDannold, N. Vykhodtseva, and K. Hynynen, "Effects of acoustic parameters and ultrasound contrast agent dose on focused-ultrasound induced blood-brain barrier disruption," Ultrasound Med. Biol. **34**, 930–937 (2008).
[5]D. L. Miller, C. Dou, and R. C. Wiggins, "Frequency dependence of kidney injury induced by contrast-aided diagnostic ultrasound in rats," Ultrasound Med Biol. **34**, 1678–1687 (2008).
[6]K. Hynynen, N. McDannold, N. Vykhodtseva, S. Raymond, R. Weissleder, F. A. Jolesz, and N. Sheikov, "Focal disruption of the blood-brain barrier due to 260-kHz ultrasound bursts: A method for molecular imaging and targeted drug delivery," J. Neurosurg. **105**, 445–454 (2006).
[7]V. Normand, D. L. Lootens, E. Amici, K. P. Plucknett, and P. Aymard, "New insight into agarose gel mechanical properties," Biomacromolecules **1**, 730–738 (2000).
[8]V. Egorov, S. Tsyuryupa, S. Kanilo, M. Kogit, and A. Sarvazyan, "Soft tissue elastometer," Med. Eng. Phys. **30**, 206–212 (2008).
[9]M. A. Borden, D. E. Kruse, C. F. Caskey, S. K. Zhao, P. A. Dayton, and K. W. Ferrarra, "Influence of lipid shell physicochemical properties on ultrasound-induced microbubble destruction," IEEE Trans. Ultrason. Ferroelectr. Freq. Control **52**, 1992–2002 (2005).
[10]C. Caskey, S. Stieger, S. Qin, P. Dayton, and K. W. Ferrarra, "Direct observation of microbubble interaction with the endothelium," J. Acoust. Soc. Am. **122**(2), 1191–1200 (2007).
[11]K. E. Morgan, J. S. Allen, P. A. Dayton, J. E. Chomas, A. L. Klibaov, and K. W. Ferrarra, "Experimental and theoretical evaluation of microbubble behavior: Effect of transmitted phase and bubble size," IEEE Trans. Ultrason. Ferroelectr. Freq. Control **47**, 1494–1509 (2000).
[12]E. A. Brujan, and A. Vogel, "Stress wave emission and cavitation bubble dynamics by nanosecond optical breakdown in a tissue phantom," J. Fluid Mech. **558**, 281–308 (2006).
[13]T. Kodama and Y. Tomita, "Cavitation bubble behavior and bubble-shock wave interaction near a gelatin surface as a study of in vivo bubble dynamics," Appl. Phys. B: Lasers Opt. **70**, 139–149 (2000).
[14]E. A. Brujan, G. S. Keen, A. Vogel, and J. R. Blake, "The final stage of the collapse of a cavitation bubble close to a rigid boundary," Phys. Fluids **14**, 85–92 (2002).
[15]J. Brunton, "High speed liquid impact," Philos. Trans. R. Soc. London, Ser. A **260**, 79–85 (1966).
[16]P. Prentice, A. Cuschieri, K. Dholakia, M. Prausnitz, and P. Campbell, "Membrane disruption by optically controlled microbubble cavitation," Nat. Phys. **1**, 107–110 (2005).
[17]S. Qin and K. W. Ferrara, "Acoustic response of compliable microvessels containing ultrasound contrast agents," Phys. Med. Biol. **51**, 5065–5088 (2006).
[18]P. A. Dayton, J. S. Allen, and K. W. Ferrara, "The magnitude of radiation force on ultrasound contrast agents," J. Acoust. Soc. Am. **112**, 2183–2192 (2002).